

SPECTRAL LINE PROFILES AND LUMINOSITIES OF ASTROPHYSICAL WATER MASERS

GERALD E. NEDOLUHA¹

Code 4030, Naval Research Laboratory, Washington, DC 20375-5000

AND

WILLIAM D. WATSON²

Departments of Physics and Astronomy, University of Illinois at Urbana-Champaign

Received 1990 September 21; accepted 1990 November 6

ABSTRACT

The spectral line narrowing and rebroadening that occurs for astrophysical masers as a function of the emergent radiative flux is calculated for the prominent, 22 GHz masing transition of water. Hyperfine structure and cross-relaxation are treated explicitly. The increased line breadths due to hyperfine structure lead to reliable, essentially model-independent upper limits to the emergent flux that tend to be lower than other estimates for these masers. For many 22 GHz masers including the outbursts in W49 and Orion which have the highest reported brightness temperatures ($\approx 10^{15}$ K), the observed line breadths are less than 0.8 km s^{-1} (FWHM). For these, the upper limit to the emergent maser flux is $T_b \Delta\Omega \gtrsim 10^{10} \text{ K sr}$ when expressed in terms of the brightness temperature T_b and the solid angle $\Delta\Omega$ for beaming.

As a result, the long-standing puzzle of the extreme brightness of the interstellar water masers is largely resolved. Their brightness is due to a high degree of beaming ($\Delta\Omega \lesssim 10^{-5} \text{ sr}$ in some cases) and not to more effective pumping. The actual maser luminosities are smaller by factors of 100 than those of certain previous assessments.

Information concerning the spectral line profiles and luminosities also bears on efforts to understand the relationship between the recently discovered water masers at millimeter and submillimeter wavelengths and the 22 GHz masers. Inferences about the strength of the magnetic field in star-forming regions based on the observed circular polarization of the 22 GHz masers are influenced, as well, by results here—by the upper limits to the radiative flux and by the conclusion that a single hyperfine component ordinarily is not dominant.

Subject headings: line profiles — masers

1. INTRODUCTION

The spectral line profiles of astrophysical masers first become narrower with increasing radiative flux (here, flux is the angular integral of the intensity) and then rebroaden when the flux is large enough that the masers become radiatively saturated (Litvak 1970). If redistribution of the excitation among the molecular velocities due to cross-relaxation is efficient, as expected, rebroadening is postponed until the radiative flux is large enough that the rate for stimulated emission exceeds the rate for cross-relaxation (Goldreich and Kwan 1974). The spectral line profiles that result are readily obtained when only single upper and lower energy levels are involved. Their application to the prominent, 22 GHz masing transition of water is, however, questionable because of the presence of hyperfine structure with splittings that are comparable with the spectral line breadth. For the three strongest hyperfine transitions, the separations in velocity units are 0.45 and 0.58 km s^{-1} between the $F = 7-6$, $6-5$, and $5-4$ components (Kukolich 1969), and the relative line strengths are 0.385:0.324:0.273, respectively. We have verified that only these three hyperfine transitions make a measurable contribution. Although a number of observational studies have focused on the spectral line profiles of the 22 GHz water masers and on the relative contributions of the various hyperfine components,

there seem to be no calculations that quantitatively deal with these issues (cf. Kwan 1974). That is the goal of the investigation here. Interpretations of a number of aspects of the observations are influenced by these calculations. This is discussed in § 4.

2. CALCULATIONS

The rate equations are solved for the populations of the various hyperfine states of the upper and lower energy levels (rotational) for the 22 GHz masing transition of the water molecule. Populations are obtained at each molecular velocity within the Maxwellian distribution of kinetic energies. As is commonly done, we use phenomenological pump rates $\lambda\phi(v)$ and decay rates Γ to represent the gains and losses due to transitions between the masing states and other molecular states. Our pump rates incorporate the usual premises that the pumping process does not favor particular molecular velocities or hyperfine states. The former premise is reflected in the pump rates by a Maxwellian distribution $\phi(v)$ of velocities v . To examine the influence of cross-relaxation (Goldreich, Keeley, & Kwan 1973; Goldreich & Kwan 1974), we include a phenomenological cross relaxation rate Γ_v such that every emission and reabsorption of an infrared photon generates a newly excited molecule at random within a Maxwellian velocity distribution and with a hyperfine state selected in proportion to the statistical weight of the state. The actual rate for redistribution in velocity is not exactly the same as for the redistribution among hyperfine states, but both are expected to be

¹ National Research Council/NRL Cooperative Research Associate, Washington, DC.

² Postal address: Department of Physics, University of Illinois at Urbana-Champaign, 1110 West Green Street, Urbana, IL 61801.

roughly the inverse lifetime of the state due to emission of infrared radiation. For simplicity, we take them to be the same and represented as Γ_v ($\approx 1 \text{ s}^{-1}$; see § 4).

Previous studies have found that the weaker three of the six hyperfine transitions have negligible influence on the maser radiation (Deguchi & Watson 1986). We have performed computations including all six for the populations as a function of molecular velocity and also find that the weaker three are unimportant. When cross-relaxation is explicitly included, the calculations are greatly simplified if the weaker three are completely ignored. We thus treat only the three stronger hyperfine transitions ($F = 7-6$, $6-5$, and $5-4$) in the calculations presented in this *Letter*. The rate equation for the number of molecules $n_i(v)$ per magnetic substrate per unit velocity in hyperfine state i ($F = 7, 6$ or 5) of the upper rotational level (6_{16}) is

$$0 = \frac{dn_i(v)}{dt} = -[\Gamma + \Gamma_v + R_{ij}(v)]n_i(v) + R_{ji}(v)n_j(v) + \phi(v) \left[\lambda_u + \left(\frac{\Gamma_v}{\Sigma g_i} \right) \int dv \Sigma g_i n_i(v) \right] \quad (1)$$

and for the number of molecules $n_j(v)$ in the hyperfine states of the lower rotational level (5_{23})

$$0 = \frac{dn_j(v)}{dt} = -[\Gamma + \Gamma_v + R_{ji}(v)]n_j(v) + R_{ij}(v)n_i(v) + \phi(v) \left[\lambda_l + \left(\frac{\Gamma_v}{\Sigma g_j} \right) \int dv \Sigma g_j n_j(v) \right]. \quad (2)$$

Steady state is an excellent approximation for the molecular populations and causes the time derivatives in equations (1) and (2) to vanish. Transitions are stimulated by the maser radiation from state i to j at a rate $R_{ij}(v)$ for molecules with velocity v along the direction in which the maser radiation propagates [$R_{ji}(v)$, for transitions from j to i]. Statistical weights and pumping rates for the upper and lower states are designated by g_u , g_l and λ_u , λ_l , respectively. The quantity that enters into the radiative transfer equation is the population difference $\Delta_{ij}(v)$ which can be expressed as

$$\Delta_{ij}(v) \equiv n_i(v) - n_j(v) = S\phi(v)/[\Gamma + \Gamma_v + \mathcal{R}_{ij}(v)], \quad (3)$$

where S is independent of velocity and is the same for all three ij pairs. The combined rate for stimulated emission at velocity v is

$$\mathcal{R}_{ij}(v) = (2v^2 k/c^2) g_i B_{ij} (g_i^{-1} + g_j^{-1}) \times \int dv T_b(v) \delta[v - v_{ij}(1 + v/c)] \Delta\Omega \quad (4)$$

in which $T_b(v)$ is the brightness temperature of the maser radiation at frequency ν , v_{ij} is the resonance frequency of the ij transition at rest, B_{ij} is the Einstein B -coefficient for the transition, δ is the delta function, and $\Delta\Omega$ is the solid angle into which the maser radiation is beamed. Though the results are insensitive to it, a beaming angle $\Delta\Omega$ must enter to relate the “intensities” (really, fluxes) calculated in the one-dimensional approximation to the observed intensities (e.g., Nedoluha & Watson 1990a).

Algebraic manipulations of the six equations of the form of equations (1) and (2) yield a solution for S ,

$$S = (\lambda_u - \lambda_l) \left\{ 1 - (\Gamma_v/2) \Sigma (c_i + c_j) \int dv \phi(v) / [\Gamma + \Gamma_v + \mathcal{R}_{ij}(v)] + [\Gamma_v/(2\Gamma + 2\Gamma_v)] \Sigma [(g_i - g_j)/(g_i + g_j)] (c_i - c_j) \times \int dv \phi(v) \mathcal{R}_{ij}(v) / [\Gamma + \Gamma_v + \mathcal{R}_{ij}(v)] \right\}^{-1}, \quad (5)$$

where $c_i = g_i/\Sigma g_i$ and $c_j = g_j/\Sigma g_j$. Equation (5) eliminates the need for a simultaneous numerical solution of the rate equations at each velocity and is thus a major simplification.

From the equation of radiative transfer, the change in brightness temperature at frequency ν and a spatial location given by z is

$$\frac{dT_b(\nu, z)}{dz} = h \int dv T_b(v) \left\{ g_7 B_{76} \Delta_{76}(v) \delta[v - c(\nu - \nu_{76})/\nu_{76}] + g_6 B_{65} \Delta_{65}(v) \delta[v - c(\nu - \nu_{65})/\nu_{65}] + g_5 B_{54} \Delta_{54}(v) \delta[v - c(\nu - \nu_{54})/\nu_{54}] \right\}. \quad (6)$$

The foregoing equations can be generalized in a straightforward manner to include spontaneous emission and bidirectional propagation.

3. RESULTS

The foregoing equations are solved numerically in the usual approximation of one-dimensional propagation for maser radiation. One-dimensional propagation is considered to be appropriate because of the strong propensity for the maser rays that have the paths with the greater amplifications to dominate.

In Figure 1, we present the primary results of the study—the spectral line breadth $\Delta\nu$ (FWHM) of the emergent maser radiation as a function of the product $T_b \Delta\Omega$ of the peak value (within the spectral line) of the brightness temperature and the solid angle for beaming. The quantity $T_b \Delta\Omega$ is proportional to the radiative flux emerging at the surface of the maser. From the foregoing equations, it is clear that the quantity that governs the intensity dependence of the spectral line profiles is the rate for stimulated emission for which a characteristic value for the 22 GHz transition is

$$R \simeq Ak T_b \Delta\Omega / 4\pi h \nu. \quad (7)$$

Here, A is the Einstein A -coefficient ($2 \times 10^{-9} \text{ s}^{-1}$) for the $6_{16}-5_{23}$ transition. For comparison, we also present calculations in which the hyperfine splitting is ignored (the two-level maser). In the two-level case, the spectral line breadths at a specific $T_b \Delta\Omega$ are proportional to the thermal, Doppler breadths v_{th} (for reference, $v_{\text{th}} = 0.6 [T/100 \text{ K}]^{1/2} \text{ km s}^{-1}$). Line breadths at other kinetic temperatures T in the two-level idealization can then readily be obtained from those in Figure 1. For other masing transitions for which the two-level approximation is valid such as the 325, 321, and 183 GHz water masers, the curve in Figure 1 is also applicable when the scale is changed so that, e.g.,

$$(T_b A \Delta\Omega / \nu \Gamma)_{321 \text{ GHz}} = (T_b A \Delta\Omega / \nu \Gamma)_{22 \text{ GHz}}, \quad (8)$$

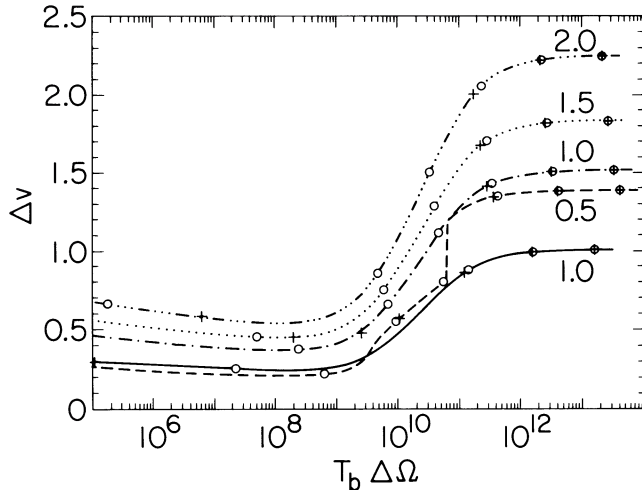


FIG. 1.—Spectral line breadth Δv km s $^{-1}$ (FWHM) for the 22 GHz, masing transition of water vs. radiative flux, expressed as the product $T_b \Delta\Omega$ (K sr) of the brightness temperature and the solid angle of the beam. The solid curve is a benchmark obtained by ignoring hyperfine structure and treating the masing as if only two energy levels are involved; the hyperfine structure is included in obtaining the other curves. Labels on the curves indicate the velocity dispersion v_{th} (FWHM) due to the kinetic temperatures of the water molecules. The lengths (arbitrary units) of the masers at various locations along the curves are indicated by open circles for the calculations with $\Gamma_v = 1$ s $^{-1}$ and $\Gamma = 0.01$ s $^{-1}$, and by crosses for $\Gamma_v = 0$ and $\Gamma = 1$ s $^{-1}$. The length is the same at all 10 of the rightmost symbols; the symbols are then located at each factor-of-10 shorter in length. For the millimeter and submillimeter masing transitions of water, the relationship between line breadth and $T_b \Delta\Omega$ can be found by scaling (see text) from that given here for the case of a transition between only two energy levels (solid curve).

where $\Gamma_>$ is the larger of Γ and Γ_v for the 321 GHz transition. The irregularities in the $v_{th} = 0.5$ km s $^{-1}$ curve with hyperfine structure are caused by the two peaks that appear at this kinetic temperature as the spectral line rebroadens (see Fig. 2). When the second peak grows to become equal to one-half of the stronger peak, it is included in giving Δv . For each choice of v_{th} (and the two-level idealization) in Figure 1, the calculations

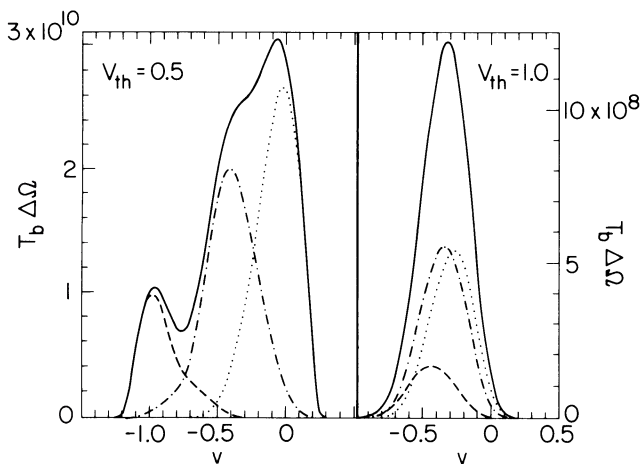


FIG. 2.—Examples of spectra line profiles for the 22 GHz masing transition of water at two kinetic temperatures indicated by v_{th} km s $^{-1}$. Maser flux expressed by $T_b \Delta\Omega$ (K sr) is shown as a function of frequency expressed as the Doppler velocity v km s $^{-1}$. The rest frequency of the $F = 7-6$ transition is at $v = 0$. The underlying curves are the contributions of each hyperfine transition ($F = 7-6$, dotted curve; $F = 6-5$, dot-dash curve; $F = 5-4$, dashed curve) to the line profile (solid curve).

are performed with and without cross-relaxation. In one case, we adopt $\Gamma_v = 1$ s $^{-1}$ and a much smaller $\Gamma = 0.01$ s $^{-1}$ —values that we consider most realistic (see Section 4). For comparison, the calculations are also performed for $\Gamma = 1$ s $^{-1}$, and cross-relaxation is assumed to be ineffective ($\Gamma_v = 0$). These curves overlap exactly in Figure 1 and are thus indistinguishable. Neither Γ nor Γ_v is expected to exceed roughly 1 s $^{-1}$ since this is the lifetime for infrared decays. If both are smaller than 1 s $^{-1}$, the curves will be displaced toward lower $T_b \Delta\Omega$. The relationship between the spectral line profile and $T_b \Delta\Omega$ thus only depends upon the larger of Γ and Γ_v . In contrast, the length of the masing region that must be traversed to achieve a particular flux (as measured by $T_b \Delta\Omega$) depends on Γ and is independent of Γ_v . To emphasize this point, we indicate the lengths of the masing regions by marks on the curves in Figure 1 for the computations with and without cross-relaxation. From Figure 1 it is clear that the effects of hyperfine structure on the spectral line breadths are significant, especially at $T \lesssim 500$ K before rebroadening occurs and in determining the line breadths after rebroadening at higher T as well.

In Figure 2, we present spectral line profiles that are computed for representative values of the key quantities (T and $T_b \Delta\Omega$). The qualitative features of spectral lines formed at higher kinetic temperatures are similar to those given for $v_{th} = 1$ km s $^{-1}$. A second peak occurs in the rebroadening regime ($R \approx \Gamma_v$) due to the $F = 5-4$ transition when the gas has a kinetic temperature near 100 K. For even modest temperatures of 250 K or so, the hyperfine components are blended well enough that the resulting spectra line appears to be completely symmetrical and indistinguishable from that which would result from a single transition, at least for unidirectional propagation. In general, the relative contributions of the three stronger hyperfine components are not in proportion to their line strengths. Their contributions also vary with the kinetic temperature and radiative flux. The frequencies at which the contributions of each of the hyperfine components reach a peak ordinarily are not at the resonances of these transitions.

Whereas the spectral line profiles for unidirectional propagation (Fig. 2) are symmetric for $v_{th} \gtrsim 1$ km s $^{-1}$, those calculated for bidirectional propagation tend to exhibit somewhat asymmetric shoulders even for thermal velocities up to $v_{th} = 2$ km s $^{-1}$. Otherwise, bidirectional masing has a negligible effect on the relationship between the spectral properties and radiative fluxes of masers presented in Figure 1.

In addition to depending upon the value of v_{th} , in principle the computed spectra depend upon the brightness temperature T_c of the background, continuum radiation that is incident upon the maser. The computations presented in Figures 1 and 2 all use $T_c \Delta\Omega = 0.1$ K sr—a value that reflects T_c of a few tens of kelvins and beaming angles $\Delta\Omega$ of about 10^{-3} sr which are considered to be plausible. Representative spectra computed for $T_c \Delta\Omega$ smaller by a factor of 10^2 are essentially unchanged; increasing $T_c \Delta\Omega$ to 10^3 K sr raises the minimum somewhat in Figure 1—by about 0.2 km s $^{-1}$ for $v_{th} = 1$ km s $^{-1}$. Such increases in Δv would tend to strengthen the main conclusions based on these computations. Spontaneous emission has also been examined and found to have no significant effect.

4. IMPLICATIONS

An estimate for the optical depths of the 22 GHz transition of astrophysical masers can be obtained from the amplification required to produce the observed brightness temperatures. The ratio of the molecular transition probabilities for the infrared

transitions in comparison with that for the 22 GHz maser transition then implies that the related infrared transitions also have large optical depths (de Jong 1973) with typical values of 10^2 – 10^3 in models for the stronger masers. This motivates our choice $\Gamma = 0.01 \text{ s}^{-1}$ for calculations in Figure 1. The decay rate Γ is the loss rate for population from the masing states and is often determined by the escape of infrared photons. Only a fraction (optical depth) $^{-1}$ of the infrared decays can escape; hence, the large reduction factor in obtaining Γ from the characteristic inverse lifetime of 1 s^{-1} for infrared emission. In contrast, under such conditions, cross-relaxation occurs at a rate comparable to the inverse lifetime for infrared emission, or $\Gamma_v \approx 1 \text{ s}^{-1}$ (Goldreich & Kwan 1974). Since rebroadening of the spectral profile occurs when the rate for stimulated emission exceeds Γ_v , the radiative flux at which rebroadening occurs is thus specified in a manner that is relatively independent of detailed models of the masers. In terms of brightness temperature, rebroadening begins at approximately $T_b \Delta\Omega = 10^9 \text{ K sr}$ (see Fig. 1). Studies for the pumping of the 22 GHz masers, especially in connection with the submillimeter water masers, indicate kinetic temperatures significantly greater than 100 K and probably near 400 K or above (e.g., Neufeld & Melnick 1990). Spectral line breadths in the neighborhood of and below 0.8 km s^{-1} (FWHM) are common for the 22 GHz masers (Moran et al. 1973; Genzel et al. 1981; Schneps et al. 1981; Fiebig & Güsten 1989). The line breadths are 0.6 km s^{-1} or smaller even for the outbursts in W49 and in Orion (Burke et al. 1972; Garay, Moran, & Hashick 1989; Matveenko 1985) which have the highest brightness temperatures ($T_b \approx 10^{15} \text{ K}$) yet reported. From Figure 1, $T_b \Delta\Omega \approx 10^{10} \text{ K sr}$ when $\Delta v \approx 0.8 \text{ km s}^{-1}$. This limit on $T_b \Delta\Omega$ would be about a factor of 10 weaker if it were obtained from a two-level calculation in which the hyperfine structure is ignored (see Fig. 1). Additional contributors to the spectral line breadth such as velocity gradients or some form of microturbulence would only raise the curves in Figure 1 and strengthen the limit on $T_b \Delta\Omega$. In addition to the evidence from pumping considerations, the smooth and symmetrical profiles from the observations provide additional evidence against kinetic temperatures as low as 100 K (see Fig. 2). Only a small fraction of the 22 GHz masers probably have $\Delta v \approx 1.5 \text{ km s}^{-1}$ which would be necessary if their profiles were fully rebroadened. For the Orion flare, Δv has been reported to be as small as 0.4 km s^{-1} —a breadth that is essentially the minimum breadth in Figure 1 for kinetic temperatures that are compatible with the pumping and with the absence of asymmetries in the line profile. Although spectral line breadths for the extensively studied OH (18 cm) masers are frequently as small as 0.1 – 0.2 km s^{-1} , those of the 22 GHz masers are rarely observed to be smaller than 0.5 km s^{-1} . It is natural to ascribe this difference to hyperfine effects in the latter and to take this as observational evidence in support of the relevance of the calculations here.

The very high brightness temperatures and inferred luminosities of the interstellar, 22 GHz masers have been a major puzzle since the VLBI observations in the early 1970s (e.g., Downes 1985; Genzel 1986). Imaginative pumping mechanisms have been proposed to generate the high maser luminosities that have seemed to be required (e.g., Strelhnikij 1984; Kylafis & Norman 1987; cf. Anderson & Watson 1990). Since the interstellar masers with the highest brightness temperatures and with many of the highest inferred luminosities must have $T_b \Delta\Omega \approx 10^{10} \text{ K sr}$ according to the foregoing, it is clear that the resolution to the puzzle of the very high bright-

ness temperatures is very small beaming angles ($\Delta\Omega \approx 10^{-5} \text{ sr}$ in some cases) and not high luminosities. The limitation on $T_b \Delta\Omega$ implies luminosities that are a factor of 100 below those of previous estimates (Reid & Moran 1981). Maser amplification between separated masing regions has been proposed to cause such beaming (Deguchi & Watson 1989). The observed cases of high linear polarization (e.g., the Orion outburst) are also easier to understand for the lower values of the maser flux (Nedoluha & Watson 1990a). Reliable information about the brightness temperatures and spectral line breadths for the extragalactic 22 GHz masers is not available. Other considerations have, however, led to the proposal that strong beaming plays a role for these, as well (e.g., Haschick et al. 1990).

Efforts to understand the pumping of the submillimeter water masers have focused on the premise that they occur in the same locations and with the same beaming angle $\Delta\Omega$, as the well-studied 22 GHz masers (Neufeld & Melnick 1990, 1991). Hyperfine effects are unimportant for these. The variation of their line breadths with maser flux is then that of a two-level transition as given in Figure 1 (with a redefinition of $T_b \Delta\Omega$ as described in § 2). The studies indicate that the 321 GHz transition of water should be less radiatively saturated than the 22 GHz maser. For the 321 GHz transition, the larger of Γ and Γ_v is at least as large as for the 22 GHz transition. The spectral line breadths of the 321 GHz masers should then tend to be narrower than those of 22 GHz masers if they are in fact in the same regions and if additional contributions to the line breadth, which could blur this difference, such as velocity gradients, are unimportant.

Certain 22 GHz observations show a definite variation in which the spectral line breadth is proportional to the inverse of the square root of the brightness temperature. Arguments have been advanced that this is a straightforward consequence of line narrowing (e.g., Rowland & Cohen 1986). No such variation is evident in Figure 1, and the origin of this striking observational relationship between the spectral line breadth and the intensity must be reexamined.

Although they are believed to be unsaturated, certain 22 GHz masers in circumstellar environments have line breadths that approach 1 km s^{-1} (Reid & Menten 1990). The calculations here indicate that, in the unsaturated regime, such breadths cannot be attributed solely to hyperfine splittings. Velocity gradients are a more likely cause.

A further impetus for clarifying the role of the various hyperfine components in the 22 GHz profile is the recent detection of circular polarization. The strengths of the magnetic fields that are inferred with the standard Zeeman interpretation and by assuming that one of the hyperfine components is dominant are the largest yet detected in star-forming regions (Fiebig & Güsten 1989). Our calculations indicate that a single component is rarely dominant. Although the Landé g -factors for the $F = 7-6$ and $6-5$ transitions differ by less than a factor of 2 (that of the $F = 5-4$ transition differs by more), the effect on the polarization caused by blending hyperfine components within a single spectral profile is unclear. Major modifications to the standard Zeeman relationship between the circular polarization and the magnetic field have been found when the stimulated emission rate is within an order of magnitude or so of the Zeeman frequency (Nedoluha & Watson 1990b). From Figure 1, the rates for stimulated emission are less likely to be high enough that such modifications are dominant if symmetric profiles with breadths less than about 0.6 km s^{-1} are chosen for study.

We are grateful to P. F. Bowers for making available unpublished observations, and to him and K. Y. Lo for helpful dis-

cussions. This research has been supported in part by the grants NASA NAGW-1104 and NSF AST 89-19614.

REFERENCES

- Anderson, N., & Watson, W. D. 1990, *ApJ*, 348, L69
 Burke, B. F., et al. 1972, *Soviet Astr.*, 16, 379
 Deguchi, S., & Watson, W. D. 1986, *ApJ*, 302, 750
 ———. 1989, *ApJ*, 340, L17
 de Jong, T. 1973, *A&A*, 26, 297
 Downes, D. 1985, in *Proc. of the Les Houches Summer School*, ed. R. Lucas, A. Omont, & R. Stora (Amsterdam: North-Holland), p. 557
 Fiebig, D., & Güsten, R. 1989, *A&A*, 214, 333
 Garay, G., Moran, J. M., & Haschick, A. D. 1989, *ApJ*, 338, 244
 Genzel, R. 1986, in *Masers, Molecules, and Mass Outflows in Star Forming Regions*, ed. A. D. Haschick (Westford, MA: Haystack Observatory), p. 233
 Genzel, R., et al. 1981, *ApJ*, 247, 1039
 Goldreich, P., Keeley, D. A., & Kwan, J. Y. 1973, *ApJ*, 182, 55
 Goldreich, P., & Kwan, J. Y. 1974, *ApJ*, 190, 27
 Haschick, A. D., Baan, W. A., Schneps, M. H., Reid, M. J., Moran, J. M., & Güsten, R. 1990, *ApJ*, 356, 149
 Kukolich, S. 1969, *J. Chem. Phys.*, 50, 3751
 Kwan, J. Y. 1974, *ApJ*, 182, 55
 Kylafis, N. D., & Norman, C. 1986, *ApJ*, 300, L73
 Litvak, M. M. 1970, *Phys. Rev. A*, 2, 2107
 Matveenko, L. K. 1985, *Soviet Astr.*, 30, 589
 Moran, J. M., et al. 1973, *ApJ*, 185, 535
 Nedoluha, G. E., & Watson, W. D. 1990a, *ApJ*, 354, 660
 ———. 1990b, *ApJ*, 361, L53
 Neufeld, D. A., & Melnick, G. J. 1990, *ApJ*, 352, L9
 ———. 1991, *ApJ*, in press
 Reid, M. J., & Menten, K. M. 1990, *ApJ*, 360, L51
 Reid, M. J., & Moran, J. M. 1981, *ARA&A*, 19, 231
 Rowland, P. R., & Cohen, R. J. 1986, *MNRAS*, 220, 233
 Schneps, M. H., Lane, A. P., Downes, D., Moran, J. M., Genzel, R., & Reid, M. J. 1981, *ApJ*, 249, 124
 Strel'nitskij, V. A. 1984, *MNRAS*, 207, 339